



# DIGITAL ACCESS TO SCHOLARSHIP AT HARVARD

## New Constraints on Methane Fluxes and Rates of Anaerobic Methane Oxidation in a Gulf of Mexico Brine Pool via In Situ Mass Spectrometry

The Harvard community has made this article openly available. [Please share](#) how this access benefits you. Your story matters.

|                          |   |
|--------------------------|---|
| <b>Citation</b>          | Wankel, Scott D., Samantha B. Joye, Vladimir A. Samarkin, Sunita Rajesh Shah, Gernot Friederich, John Melas-Kyriazi, and Peter R. Girguis. 2010. New constraints on methane fluxes and rates of anaerobic methane oxidation in a Gulf of Mexico brine pool via in situ mass spectrometry. <i>Deep Sea Research Part II: Topical Studies in Oceanography</i> 57(21-23): 2022-2029. |
| <b>Published Version</b> | <a href="https://doi.org/10.1016/j.dsr2.2010.05.009">doi:10.1016/j.dsr2.2010.05.009</a>   |
| <b>Accessed</b>          | February 19, 2015 10:53:39 AM EST   |
| <b>Citable Link</b>      | <a href="http://nrs.harvard.edu/urn-3:HUL.InstRepos:10136320">http://nrs.harvard.edu/urn-3:HUL.InstRepos:10136320</a>   |
| <b>Terms of Use</b>      | This article was downloaded from Harvard University's DASH repository, and is made available under the terms and conditions applicable to Open Access Policy Articles, as set forth at <a href="http://nrs.harvard.edu/urn-3:HUL.InstRepos:dash.current.terms-of-use#OAP">http://nrs.harvard.edu/urn-3:HUL.InstRepos:dash.current.terms-of-use#OAP</a>                            |

*(Article begins on next page)*

1 **New constraints on methane fluxes and rates of anaerobic**  
2 **methane oxidation in a Gulf of Mexico brine pool via *in situ***  
3 **mass spectrometry**

4  
5  
6  
7 **Scott D. Wankel<sup>1</sup>, Samantha B. Joye<sup>2</sup>, Vladimir A. Samarkin<sup>2</sup>, Sunita R. Shah<sup>3</sup>,**  
8 **Gernot Friederich<sup>4</sup>, John Melas-Kyriazi<sup>5</sup>, and Peter R. Girguis<sup>1\*</sup>**

9  
10  
11  
12  
13  
14  
15  
16  
17  
18  
19  
20  
21  
22  
23  
24  
25  
26  
27  
28  
29  
30  
31  
32  
33  
34  
35  
36  
37  
38 <sup>1</sup>Department of Organismic and Evolutionary Biology, Harvard University, Cambridge,  
39 MA 02138.

40 \*Corresponding author: [pgirguis@oeb.harvard.edu](mailto:pgirguis@oeb.harvard.edu)

41 <sup>2</sup>Department of Marine Sciences, University of Georgia, Athens, GA 30602-3636

42 <sup>3</sup>US Naval Research Laboratory, Washington DC 20375

43 <sup>4</sup>Monterey Bay Aquarium Research Institute, Moss Landing, CA

44 <sup>5</sup>Stanford University, Stanford, CA 94305

45

46 **Abstract**

47 Deep sea biogeochemical cycles are, in general, poorly understood due to the  
48 difficulties of making measurements *in situ*, recovering samples with minimal  
49 perturbation and, in many cases, coping with high spatial and temporal heterogeneity. In  
50 particular, biogeochemical fluxes of volatiles such as methane remain largely  
51 unconstrained due to the difficulties of accurate quantification *in situ* and the patchiness  
52 of point sources such as seeps and brine pools. To better constrain biogeochemical fluxes  
53 and cycling, we have developed a deep sea *in situ* mass spectrometer (ISMS) to enable  
54 high-resolution quantification of volatiles *in situ*. Here we report direct measurements of  
55 methane concentrations made in a Gulf of Mexico brine pool located at a depth of over  
56 2300m. Concentrations of up to 33mM methane were observed within the brine pool,  
57 while concentrations in the water directly above were three orders of magnitude lower.  
58 These direct measurements enable the first accurate estimates of the diffusive flux from a  
59 brine pool, calculated to be  $1.1 \pm 0.2 \text{ mol m}^{-2} \text{ yr}^{-1}$ . Integrated rate measurements of  
60 aerobic methane oxidation in the water column overlying the brine pool were  $\sim 320 \text{ } \mu\text{mol}$   
61  $\text{m}^{-2} \text{ yr}^{-1}$ , accounting at most for just 0.03% of the diffusive methane flux from the brine  
62 pool. Calculated rates of anaerobic methane oxidation were 600 to 1200  $\mu\text{M yr}^{-1}$ , one to  
63 two orders of magnitude higher than previously published values of AOM in anoxic  
64 fluids. These findings suggest that brine pools are enormous point sources of methane in  
65 the deep sea, and may, in aggregate, have a pronounced impact on the global marine  
66 methane cycle.

67

67 **Introduction**

68 **1.1. Global importance of methane**

69 The marine methane cycle has been the subject of much investigation in recent  
70 years, in large part due to burgeoning interest and concern over deep ocean methane  
71 hydrates. The deep ocean methane reservoir represents an enormous and dynamic pool  
72 of carbon likely exceeding reserves of conventional oil and gas (Collett and Kuuskraa,  
73 1998). In deep ocean regions, characterized by low temperatures, high pressure and  
74 sufficient methane concentration, methane exists largely in the solid form of a gas  
75 hydrate (Kvenvolden, 1993). Methane seeps and associated gas hydrates have been  
76 identified along many passive and active continental margins (Kvenvolden and Lorenson,  
77 2008). Because the destabilization of hydrates is sensitive to increases in temperature or  
78 decreases in pressure, it has been postulated that increases in mean global temperatures  
79 might trigger a release of methane into the ocean and atmosphere. A significant release  
80 of methane into the atmosphere could ultimately lead to a catastrophic greenhouse effect;  
81 this mechanism has been invoked as an explanation for past deglaciation events (Dickens,  
82 2003; Sloan *et al.*, 1992; Zachos *et al.*, 2001).

83 Despite recent, numerous studies of methane hydrates, modern fluxes of methane  
84 from the deep sea into surface waters and ultimately the atmosphere are very poorly  
85 constrained. Estimates of methane flux have been aided, to some degree, by recent  
86 advances in our understanding of marine microbiological influences on the global  
87 methane cycle. Aspects of the marine methane cycle remain largely unconstrained due to  
88 limitations in methods and technologies that enable accurate assessment of methane

89 concentration and flux – as well as rates of biological methanogenesis or methanotrophy.  
90 Pressure and temperature have a pronounced effect on methane solubility. As such,  
91 upon retrieval of methane-saturated waters or hydrate-rich sediments from the deep  
92 ocean, methane rapidly outgasses to the atmosphere. Thus, it has been challenging to  
93 constrain flux and microbial activity *in situ*, under environmentally relevant conditions.  
94 Because previous data have shown that methane oxidation, both aerobic and anaerobic,  
95 are the largest methane sinks in marine environments (Reeburgh, 2007), understanding  
96 what controls methane oxidation -including concentration and abiotic flux- are paramount  
97 to understanding global methane dynamics.

98       To better constrain the methane flux in chemically reducing environments – and  
99 ultimately to quantify the influence of biotic and abiotic processes on the methane cycle –  
100 we employed a newly developed *in situ* mass spectrometer (ISMS) to conduct direct  
101 measurements of methane concentration which - in concert with shipboard  
102 microbiological measurements - were used to generate more robust estimates of diffusive  
103 flux and net methane oxidation rates in a newly discovered brine pool in the Gulf of  
104 Mexico.

## 105 **2. Geologic Setting**

106       Along the continental shelf in the Gulf of Mexico, massive reservoirs of liquid  
107 and gaseous hydrocarbons lie buried beneath kilometers of sediment accumulated from  
108 the Mississippi River drainage basin. Due to compression and dewatering of the  
109 overlying sediments, underlying evaporite deposits have undergone plastic deformation  
110 resulting in salt-diapir driven tectonic activity (Kennicutt *et al.*, 1988). The resulting  
111 system of fractures and faults provides conduits for the emission of hydrocarbons to the

112 seafloor via seepage (Roberts and Carney, 1997). Hydrocarbon seeps are often  
113 characterized by abundant chemosynthetic based macro- and microfaunal communities  
114 including tubeworms, mussel beds, and bacterial mats which thrive on the reduced  
115 organic compounds emanating from below (Fisher *et al.*, 2007; MacDonald *et al.*, 1990;  
116 MacDonald *et al.*, 2003). In addition, hypersaline brine fluids seep from the seafloor in  
117 many locations (MacDonald *et al.* 1990; Joye *et al.* 2005, 2009). Previous studies have  
118 provided insight into the geochemical composition of these brine pools, though to date  
119 volatile flux and net rates of methane oxidation remain poorly constrained due to the  
120 challenges in quantification resulting from off-gassing (at *in situ* pressures and  
121 temperatures relevant here, methane saturation is  $\sim 174 \text{ mmol kg}^{-1}$  (Duan and Mao,  
122 2006)). Accurate sampling of fluids with high gas content using conventional methods  
123 (e.g., Niskin Bottles) has thus proven impractical for volatiles.

124         The brine pool characterized in this study (AC601) is located in the Alaminos  
125 Canyon lease block 601 (26° 23.53 N; 94° 30.85 W; Roberts *et al.* this issue; (Roberts *et*  
126 *al.*, 2007). The brine pool is estimated to be  $\sim 250\text{m}$  in diameter and approximately 2334  
127 meters below sea surface. This brine pool was visited during expeditions on board the  
128 *RV Ronald H. Brown* using the *DSV Jason II* during expeditions from May 6 through  
129 June 4, 2006 and June 3 through July 6, 2007 (see Roberts *et al.*, this issue), for further  
130 description of the expeditions and site locations). Discrete geochemical measurements of  
131 this brine pool were made during the 2006 and 2007 expedition, while deployment of the  
132 ISMS was carried out during the 2007 expedition.

### 133 3. Methods

#### 134 3.1. *Fundamentals of Membrane Inlet Mass Spectrometry/ISMS*

135 Over the past five decades, the use of membrane inlet mass spectrometry (MIMS)  
136 has proven to be a powerful tool for measuring complex mixtures of dissolved gases in  
137 both industrial and laboratory settings (Johnson *et al.*, 2000; Ketola *et al.*, 2002). MIMS  
138 represents an optimal technique for mixed environmental gas analysis, having a high  
139 degree of sensitivity and precision, with minimal sample perturbation (Kana *et al.*, 1994).  
140 MIMS has been used over the past several decades to measure and monitor a wide range  
141 of dissolved gases in aquatic and terrestrial environments, including studies of bacterial  
142 mats, peat bogs, estuarine sediments, forest soils, and tree canopies to name a few  
143 (Hemond, 1991; Kana *et al.*, 1998; Lloyd *et al.*, 1986; Lloyd *et al.*, 1998). MIMS has  
144 also been used to study metabolite flux during shipboard high-pressure experiments (e.g.,  
145 (Girguis *et al.*, 2002; Girguis *et al.*, 2000). MIMS has also emerged as an important tool  
146 for analyzing dissolved gases in seawater, (e.g. dissolved gases in surface waters  
147 analyzed continuously shipboard;(Kaiser *et al.*, 2005; Tortell, 2005a; Tortell, 2005b) and  
148 more recently for *in situ* marine surface waters (Bell *et al.*, 2007; Camilli and Hemond,  
149 2004; Kaiser *et al.*, 2005; Tortell, 2005b, c).

150 The recent adaptation of MIMS to *in situ* environmental analyses demonstrates  
151 the utility of such an instrument operating while underway at sea – allowing the continual  
152 monitoring of many gas species in real time. This approach allows highly accurate  
153 monitoring of spatially explicit biogeochemical changes. For example, changes in O<sub>2</sub>/Ar  
154 indicate changes in net community production in ocean surface waters in different  
155 regions of the eastern equatorial Pacific (Kaiser *et al.*, 2005). Additionally, N<sub>2</sub>/Ar has

156 been used to identify areas of active denitrification (e.g., N<sub>2</sub> production) in seasonally  
157 oxygen-depleted bottom waters via MIMS in Saanich Inlet (Tortell, 2005b). Underway  
158 shipboard trace gas analysis has also shed light on dynamics of dimethylsulfide (Tortell,  
159 2005a).

160         Given the apparent utility of real-time quantification by MIMS, we aimed to  
161 develop a MIMS that would achieve comparable performance in waters deeper than 1000  
162 meters. Currently, investigation of deep water samples still generally requires the  
163 collection of individual samples and shipboard analysis (e.g., Tortell, 2005b), risking  
164 contamination and/or degassing. Furthermore, individual sample collection and analysis  
165 can often result in delays between sampling and data interpretation. Our understanding  
166 of deep-sea biogeochemistry would greatly benefit from real-time, *in situ* dissolved gas  
167 analysis. Here we present results from a real-time *in situ* membrane inlet mass  
168 spectrometer designed to A) operate at depths up to 450 atmospheres of pressure, B)  
169 provide real-time data to the user (when used on human occupied submersibles or  
170 remotely operated vehicles), and C) enable sampling with high spatial and temporal  
171 resolution using an *in situ* pumping system.

### 172 **3.2. ISMS Design and Calibration**

173         This ISMS consisted of three primary sub-systems: 1) a high-pressure membrane  
174 inlet (Fig. 1a) with a small volume seawater pumping system;, 2) a quadrupole mass  
175 spectrometer (Fig. 1e, f) and oil-less vacuum pumping system (Fig. 1 d, g); and 3) an  
176 underwater housing (either a 2000 meter-rated aluminum 3300 alloy housing, or a 4500  
177 meter rated 6AL-4V titanium housing, both of which are approximately 120 cm in length  
178 and 24 cm in diameter). The membrane inlet assembly consisted of a circular sheet



179 (0.625 in. diameter) of polydimethylsiloxane (PDMS) membrane structurally backed by  
180 an integrated woven fiber (Franatech, Germany). This pliable membrane material was  
181 supported by a sintered stainless steel frit (5 $\mu$ m pore size, Applied Porous Materials,  
182 Tariffville, CT), which was in turn supported by the titanium body of the inlet housing.  
183 Sample water was pumped through the inlet housing assembly (2ml internal volume) at a  
184 flow rate of  $\sim$ 3ml/min using a small solenoid pump (The Lee Company, Westbrook, CT),  
185 which was controlled by an adjustable timing circuit located inside of the pressure  
186 housing.

187         The membrane assembly was connected to a Stanford Research Systems Residual  
188 Gas Analyzer (SRS RGA100) via standard vacuum flanges. Within the vacuum system,  
189 a pressure of  $\sim$  10e<sup>-5</sup> Torr was maintained by a turbo-molecular pump (model: ATH 31+;  
190 Alcatel, France) backed by a diaphragm roughing pump (model: ANDC83.4; KNF-  
191 Neuberger, Trenton, NJ). Open source electron impact ionization was carried out with a  
192 thoriated iridium wire filament. The mass spectrometer and pumps were protected from  
193 membrane failure by a high-pressure / high-vacuum solenoid valve (Circle Seal, Inc.,  
194 Corona, CA), which is actuated upon intrusion of water. The entire mass spectrometer  
195 assembly was housed in one of the aforementioned housings. 24 VDC power and two  
196 independent RS-232 channels (for serial communications with the turbo pump control  
197 board and continuous feedback from the RGA analyzer) were supplied via a wet-connect  
198 underwater cable (SubConn, Inc., North Pembroke, MA). In this configuration, real time  
199 monitoring of fluid chemistry is achievable during submersible or ROV operations,  
200 which allows for informed site selection for fluid measurements as well as adaptive  
201 sampling of biological specimens.

202 To conduct the benchtop high-pressure calibrations (Fig. 2), model 110A HPLC  
203 pumps (Beckman-Coulter, Fullerton, CA) were used to deliver calibrated solutions past  
204 the membrane surface at various flow rates and pressures. Hydrostatic pressure against  
205 the membrane inlet was manually controlled with a backpressure valve (StraVal Valve,  
206 Garfield, NJ) and monitored with high pressure gauges. Various calibration solutions  
207 were used including air-sparged DI water or seawater, degassed distilled water and/or  
208 seawater equilibrated with gas mixtures of interest (e.g., CH<sub>4</sub>), including the use of a high  
209 pressure equilibration system for generating very high CH<sub>4</sub> concentrations (Fig. 2). A  
210 gas chromatograph (HP 5890 Series II plus with a TCD) outfitted with a custom gas  
211 extractor (Childress *et al.*, 1984) designed for quantification of rapidly degassed seawater  
212 samples was used to obtain independent analyses of dissolved methane concentrations,  
213 while previously described equations of state were used to calculate dissolved methane  
214 concentrations at very high pressures (Duan and Mao, 2006) (Fig. 2b). During lab  
215 experiments, relative changes in signal intensity were proportional to changes in the  
216 permeation of gas through the membrane (either due to changes in permeate  
217 concentration or changes in the permeability coefficient). We and others have observed  
218 that changes in hydrostatic pressure can have an influence on permeation of gases  
219 through membrane materials, in particular PDMS, interpreted to be caused by  
220 compression of the membrane pore space through which analyte gas passes (Bell *et al.*,  
221 2007). A change in the relationship between dissolved gas concentration and signal  
222 intensity was observed during large changes in hydrostatic pressure (Fig. 2a). To account  
223 for this response, we conducted calibrations using methane dissolved in seawater over a  
224 range of *in situ* pressures and used these results to develop an empirical correction as

225 previously described (Bell et al., 2007). While this approach corrects for implicit  
226 changes in membrane behavior, it should be noted that the ISMS dataset presented here is  
227 comprised entirely of fluids sampled at a relatively constant depth ( $\sim 2330\text{m} \pm 2$  (233  
228 bar)) and temperature and as such effects due to differential pressure or temperature  
229 among the samples collected were negligible. Based on benchtop calibrations, the  
230 accuracy of the ISMS methane concentrations in the configuration described here was  $\pm$   
231 11%, primarily due to the correction required for the pressure effects on the PDMS  
232 membrane (accuracy is improved through the use of alternate membrane material (e.g.  
233 Teflon AF)). Notably, however, the precision of the ISMS measurements is much better  
234 than this and, based on benchtop calibrations, is within  $\pm 1\%$ .

### 235 **3.3. *Water Column Methane and Oxygen Concentration***

236 To determine brine pool and seawater column methane concentrations, a CTD  
237 rosette was lowered into the brine pool, using sonar to identify the brine pool as the  
238 rosette approached the bottom. Niskin bottles were tripped during descent to prevent  
239 contamination of bottles as gas came out of solution during the rosette's ascent. Two  
240 bottles were tripped in the brine pool itself, while two were tripped 1 meter above the  
241 brine-seawater interface (the interface was confirmed by the real-time conductivity  
242 signal). After securing the rosette on deck, water samples were immediately transferred  
243 to 1-liter PET-G bottles using gas-impermeable tubing. Bottles that were tripped in the  
244 brine were substantially over-pressured and not suitable for gas quantification (though  
245 samples were transferred to the PET-G bottles for rate measurements). A second sample  
246 was transferred to a 250 mL BOD bottle for determination of dissolved oxygen using a  
247 high sensitivity Orion<sup>®</sup> oxygen electrode. Methane was extracted using an adaptation of

248 the sonication/vacuum extraction technique (Suess *et al.*, 1999) followed by gas  
249 chromatography for quantification. Prior to dissolved gas extraction, samples were  
250 stored at bottom water temperature (4 °C). Two individual samples were analyzed from  
251 each rosette bottle.

### 252 **3.4. ISMS Deployments and Determining Brine Pool Methane Concentrations**

253 Upon reaching the brine pool, the submersible took care not to disturb the brine-  
254 seawater interface. Using the ROV manipulator, the ISMS sample inlet was positioned  
255 and held in place until the ISMS response reached steady state from which *in situ*  
256 concentrations of CH<sub>4</sub> were calculated. A total of five independent sets of measurements  
257 were made, beginning with two just above the brine fluid and three at depths of  
258 approximately 5, 20 and 80 cm into the fluid (Figs. 3 and 4).

### 259 **3.5. Methane Oxidation Rates**

260 Aerobic methane oxidation occurs according to the following stoichiometry:



262 Accordingly, aerobic methane oxidation rates were determined by incubating samples  
263 with C<sup>3</sup>H<sub>4</sub> and tracking the production of <sup>3</sup>H<sub>2</sub>O (Carini *et al.*, 2005; Valentine *et al.*,  
264 2001). Typically, triplicate live and dead (Hg killed; i.e. samples were amended with  
265 HgCl<sub>2</sub> to arrest all biological activity) samples from each depth were incubated for 36  
266 hours at *in situ* temperatures. Unreacted C<sup>3</sup>H<sub>4</sub> tracer was removed by purging samples  
267 with water-saturated CH<sub>4</sub> and the oxidation product, <sup>3</sup>H<sub>2</sub>O, was quantified by liquid  
268 scintillation counting (Carini *et al.*, 2005).

269 In general, marine anaerobic methane oxidation in hydrocarbon seeps and brine  
270 pools is coupled to sulfate reduction, with the net reaction:



272 Anaerobic methane oxidation rates were also determined by incubating samples with  
273  $^{14}\text{CH}_4$  and tracking the production of  $^{14}\text{CO}_2$  (as in Joye *et al.*, 1999; Valentine *et al.*,  
274 2001). Triplicate live and dead (Hg killed) samples from the surface (~20 cm) and sub-  
275 surface (~100 cm) brine were incubated for 48 hours at *in situ* temperatures. Unreacted  
276  $^{14}\text{CH}_4$  tracer was removed by purging with water-saturated  $\text{CH}_4$  and the  $^{14}\text{CO}_2$  oxidation  
277 product was quantified following acid extraction and trapping on a phethylamine wick,  
278 followed by liquid scintillation counting (Carini *et al.*, 2005).

### 279 3.6. *Sulfate Reduction Rates*

280 Samples for sulfate reduction were collected into gas tight glass tubes, amended  
281 with radiotracer ( $^{35}\text{SO}_4^{2-}$ ) and incubated for 24 hours (as in Joye *et al.*, 2004; Orcutt *et al.*,  
282 2005). For each depth, triplicate samples were incubated along side controls (killed at  
283 time zero). After incubation, samples were transferred from the tubes to 50 ml centrifuge  
284 tubes and mixed with 20% zinc acetate. Samples were processed and rates calculated as  
285 presented in Orcutt *et al.* (2005).

### 286 3.7. *Major Ion chemistry*

287 Concentrations of major ions ( $\text{SO}_4^{2-}$ ,  $\text{Cl}^-$ , dissolved inorganic carbon (DIC),  
288 dissolved organic matter (DOC and DON) and dissolved inorganic nitrogen ( $\text{NH}_4^+$ ,  $\text{NO}_2^-$   
289 and  $\text{NO}_3^-$ ) were determined using previously reported methods (see (Joye *et al.*, 2004)  
290 and Joye *et al.* this volume and references therein).

## 291 4. Results

### 292 4.1. *General geochemical composition of brine pool AC601*

293 Geochemical data on the waters collected from the brine pool are given in Table  
294 1. The waters of the brine pool were anoxic ( $O_2 < 2\mu\text{M}$ ) with a pH of  $\sim 6.3$ . Salinities  
295 were substantially elevated above seawater at 82 and 92 for the 20 and 100 cm depths,  
296 respectively, with chloride measuring 1366 and 1533 mM at each depth. Water from  
297 both depths was highly enriched in dissolved inorganic carbon (DIC; 11.2 mM at 20 cm,  
298 12.8 mM at 100 cm). Sulfate concentrations were lower than seawater, decreasing with  
299 depth into the pool (Fig 4). Dissolved inorganic nitrogen was dominated by very high  
300  $\text{NH}_4^+$  (1750 and 2195  $\mu\text{M}$ , 20 and 100 cm, respectively), with  $\text{NO}_3^-$  disappearing sharply  
301 in the top meter of the brine. The dissolved organic matter content was also high with a  
302 low C:N of  $\sim 4.6$  suggesting the importance of autochthonous production within the brine  
303 waters.

### 304 4.2. *Water Column and Brine Pool $\text{CH}_4$ Oxidation and $\text{SO}_4^{2-}$ Reduction Rates*

305 Aerobic methane oxidation rates measured in the water column above the brine  
306 pool from depths of 300m to 2313m (or heights above the brine pool from 0 to 2013m)  
307 ranged from 0.00 to  $6.33 \pm 0.9 \text{ pmol L}^{-1} \text{ d}^{-1}$  (hereafter  $\text{pM d}^{-1}$ ) (Fig 4). The aerobic  
308 methane oxidation rate in the sample taken from directly above ( $\sim 3\text{m}$ ) the brine pool  
309 (2328m) was significantly higher,  $129.6 \pm 18.2 \text{ pM d}^{-1}$ , than rates at any other depth.  
310 Using the methane concentrations determined via gas chromatography and the  
311 empirically derived oxidation rates, we calculate an integrated methane oxidation rate in  
312 the water column above the brine pool of  $320 \mu\text{mol m}^{-2} \text{ yr}^{-1}$

313            Within the brine pool, two samples (20cm and 100cm) were retrieved and used  
314 for sulfate reduction and anaerobic oxidation of methane (AOM) rate measurements  
315 (Table 2). Methane concentrations measured in the bottles used for the rate  
316 measurements were 454 and 1320  $\mu\text{M}$ , respectively (Table 1), giving rates at these depths  
317 of  $78.8 \pm 7.6$  and  $62.1 \pm 13.1 \text{ nmol L}^{-1} \text{ d}^{-1}$ , respectively. Sulfate concentrations in the  
318 brine were depleted relative to seawater with concentrations of 20 and 16mM at 20cm  
319 and 100cm, respectively. Sulfate reduction rates were 107 and 50 nmoles per liter per  
320 day (hereafter  $\text{nM d}^{-1}$ ) at 20cm and 100cm, respectively, and were comparable to the rates  
321 of AOM on a per mole basis. As mentioned above, these oxidation rates were measured  
322 using water taken from CTD rosette bottles, which, when sampling gas-charged waters,  
323 are subject to outgassing and gas phase exchange during recovery. Thus, these rates are  
324 considered to be conservative estimates of anaerobic methane oxidation. *In situ* methane  
325 oxidation rates are expected to be higher as methane concentrations increase (i.e., on a  
326 first order basis up to  $k_{\text{max}}$ ) and are calculated below.

#### 327 **4.3.    *Water Column and Brine Pool Methane Concentrations***

328            Methane concentrations measured in the water column (Fig 4) directly above the  
329 brine pool ranged from 30nM to 70nM at depths between 2000 and 300m, representing  
330 concentrations that were 15 to 32 times that of atmospheric equilibrium and underscoring  
331 the transport of methane from below. At depths below 2000m, closer to the brine pool,  
332 concentrations increased sharply and ranged from 111 nM to 24  $\mu\text{M}$ . Methane  
333 concentrations, as measured by the ISMS approximately 5 cm above the brine  
334 fluid/seawater interface near the shore of the pool and 1 cm above the brine  
335 fluid/seawater interface in the center of the brine pool were 180 and 590  $\mu\text{M}$ ,

336 respectively. Approximately 1m above the brine surface, the ISMS-measured methane  
337 concentration was approximately  $\sim 35 \mu\text{M}$ , which is in general agreement with the  
338 methane concentrations measured in the CTD rosette at this depth ( $24 \mu\text{M}$ , well below  
339 the saturation of methane at one atmosphere, so these particular Niskin measurements are  
340 not compromised by off gassing, see Fig. 4). Concentrations at depths of 5, 20 and 80cm  
341 into the brine fluid near the center of the pool were orders of magnitude higher (Fig 4)  
342 with values of 14.3, 20.3 and 33.3 mM, respectively ( $\pm 2\%$ ), and more than an order of  
343 magnitude in excess of concentrations measured with Niskin sampling (see Table 1).

## 344 **5. Discussion**

### 345 **5.1. *In situ rates of brine pool anaerobic methane oxidation***

346 The *in situ* rates of AOM reported here exceed values in other anoxic waters by at  
347 least one to two orders of magnitude. Our measured rates of AOM from two sampling  
348 depths allowed calculation of first order rate constants of  $0.063$  and  $0.017 \text{ yr}^{-1}$  from  
349 depths of 20cm and 80cm, respectively. Coupling the *in situ* methane concentration  
350 measurements from the ISMS to the aforementioned rate constants yields estimates of the  
351 actual rates of AOM of  $1285 \pm 125$  and  $572 \pm 121 \mu\text{M yr}^{-1}$  at the depths of 20 and 80cm  
352 in the brine pool, respectively. To the best of our knowledge, these AOM rates are by far  
353 the highest documented in an anoxic water body. Whereas there has been some evidence  
354 that AOM is inhibited by high chloride concentrations (e.g.,(Joye *et al.*, 2009; Oren,  
355 2002)), our data (Tables 1 and 2) suggest that moderately high salinities may in fact not  
356 be inhibitory to AOM and that coupled sulfate reduction and AOM may yet play an  
357 important role in many Gulf of Mexico hydrocarbon/brine environments.



358 Many studies have measured AOM in deep sea environments with high  
359 concentrations of methane, and the highest rates are generally found within sediments,  
360 particularly hydrate-influenced sediments (e.g., (Devol, 1983; Girguis *et al.*, 2003; Joye  
361 *et al.*, 2004; Reeburgh, 1980)). Indeed, far fewer studies have measured AOM occurring  
362 in anoxic water columns, and the rates reported in these studies are generally much lower  
363 than sediment rates (as is the case with most biogeochemical processes primarily due to  
364 microbial density being substantially higher in sediments). Rates of AOM measured in  
365 the anoxic waters of the Cariaco Basin ( $\sim 1.5 \mu\text{M yr}^{-1}$ ; Ward *et al.*, 1987), Saanich Inlet  
366 ( $7.3 \mu\text{M yr}^{-1}$ ; Ward *et al.*, 1989) and the Black Sea ( $0.6 \mu\text{M yr}^{-1}$ ; Reeburgh *et al.*, 1991)  
367 were all orders of magnitude lower than those observed in this study. Joye et al (1999)  
368 measured rates as high as  $17.5 \mu\text{M yr}^{-1}$  in the bottom waters of alkaline, saline Mono  
369 Lake. Notably, these rates were measured during a period when the lake waters were  
370 well mixed. More recent data collected during a period of extended meromixis in Mono  
371 Lake exhibit substantially higher rates of AOM (up to  $365 \mu\text{M yr}^{-1}$ ) (Joye *et al.*,  
372 submitted).

373 The rates of AOM presented here are also consistent with the extremely high *in*  
374 *situ* concentrations occurring at these depths. Turnover times of methane in the anaerobic  
375 brines were on the order of 16 to 58 years, more than long enough to maintain supply of  
376  $\text{SO}_4^{-2}$  via diffusion. Such long turnover times also might suggest that supply to the  
377 overlying water via diffusion is likely to be a substantial methane sink relative to removal  
378 by AOM (or aerobic oxidation at the brine-seawater interface) in similar brine pool  
379 environments. Indeed, given that the rate constants were lower than many other  
380 comparable environments, the rates presented represent a conservative estimate and, as

381 previously mentioned, the rate constants would likely increase at the higher methane  
382 concentrations found *in situ*.

### 383 **5.2. *Estimates of CH<sub>4</sub> flux from the brine pool***

384 Research on deep-sea fluxes and transformations of biological compounds is  
385 constantly challenged by the need to sample at extreme temperatures, depths and  
386 pressures. Measurement of these compounds *in situ* provides more rigorous constraints  
387 on their fluxes and transformation rates. In the context of the current study, the *in situ*  
388 mass spectrometer allowed direct measurement of methane concentrations in a gas-  
389 charged brine pool. These concentration measurements were used to calculate a diffusive  
390 flux of methane from the brine pool into the overlying water column of  $1.1 \pm 0.2 \text{ mol m}^{-2}$   
391  $\text{yr}^{-1}$ , illustrating the magnitude of methane flux from benthic environs into the overlying  
392 mixed layer (discussed in detail below).

393 Specifically, discrete *in situ* measurements taken over a depth profile across the  
394 seawater-brine interface provide a context for calculating diffusive geochemical fluxes of  
395 methane into the overlying water column. This approach has been used in numerous  
396 studies for estimating the mass transfer (e.g., fluxes) of solutes from one region into  
397 another. Brine pools such as AC601 are generally very quiescent in nature with fluid  
398 advection playing a small role in controlling fluxes (Joye *et al.*, 2005; Joye *et al.*, 2009).  
399 In these locations, where diffusion is the dominant mode of mass transfer, Fick's first law  
400 is used to make first order estimates of the diffusive flux based on the measured  
401 concentration gradients. The range of possible flux values is estimated based on error in  
402 the spatial resolution of the gradient (i.e., since high precision positioning of the sampling  
403 wand was not possible, we estimate the potential vertical position  $\pm 10\text{cm}$ ). Moreover,

404 we adopted a value of  $1.38e^{-5} \text{ cm}^2 \text{ s}^{-1}$  for the diffusion coefficient of methane in seawater  
405 adjusted for the average viscosity of the brine using the Stokes-Einstein relationship  
406 (Mao and Duan, 2008; Sahores and Witherspoon, 1970).

407 Even with our lower-bound estimate of diffusive methane flux ( $1.1 \text{ mol m}^{-2} \text{ yr}^{-1}$ ),  
408 water column integrated methane oxidation rates (Fig. 4) measured directly above the  
409 brine pool ( $\sim 320 \mu\text{mol m}^{-2} \text{ yr}^{-1}$ ) indicate that only a very small fraction of methane  
410 escaping the brine pool is biologically consumed in the overlying water column (0.02 to  
411 0.03%). While it is likely that lateral advection plays a large role in the disconnect  
412 between brine pool flux and water column methane oxidation rates above the brine, upper  
413 water column concentrations are nonetheless  $>10$  times that of methane in equilibrium  
414 with the atmosphere, confirming the transport of methane from depths  $>2000\text{m}$  into the  
415 mixed layer which easily escapes, un-oxidized, into the atmosphere.

416 Our estimates of diffusive methane flux should be taken as a lower bound on flux  
417 from environments such as Gulf of Mexico brine pools. They also underscore the value  
418 of *in situ* measurement for constraining methane fluxes. For example, other studies  
419 (Lapham *et al.*, 2008; Schmidt *et al.*, 2003) have modeled diffusive and/or advective  
420 fluxes from brine seep environments by comparing profiles of a non-conservative solute  
421 (e.g., methane) to conservative solutes (e.g., chloride, temperature). Using a 1-D reaction  
422 transport model together with chloride and methane profiles, advective methane fluxes of  
423 up to  $2 \text{ mol m}^{-2} \text{ yr}^{-1}$  were estimated from brine-influenced sediments characterized by a  
424 strong advective flow (Lapham *et al.*, 2008). However, these calculated fluxes were  
425 based on methane concentrations from sediment cores that had degassed upon collection,  
426 and were thus substantially lower than methane concentrations *in situ*. In another study,

427 Solomon et al. (2008) employed osmotic samplers demonstrating that net seafloor  
428 methane fluxes range from  $0.89 \text{ mol m}^{-2} \text{ yr}^{-1}$  from a mussel bed environment up to 29  
429  $\text{mol m}^{-2} \text{ yr}^{-1}$  from a bacterial mat environment. Hereto, because methane concentrations  
430 could not be reliably determined at *in situ* pressure and temperature, fluxes were  
431 calculated assuming that porewater was in equilibrium with methane hydrate under *in situ*  
432 conditions. However, others have shown that methane in sediments around hydrate can  
433 be far from saturated (Lapham *et al.*, pers. comm.), which would result in much lower  
434 flux estimates. Future studies should aim to couple *in situ* methane measurements with  
435 direct fluid flow measurements to better constrain the contribution of advective flux to  
436 water column methane flux.

## 437 **6. Summary and Conclusions**

438 Our calculated *in situ* AOM rates, using empirically derived rate constants, are  
439 higher than those previously published by one to two orders of magnitude. The diffusive  
440 flux was estimated to range as high  $1.8 \text{ mol m}^{-2} \text{ yr}^{-1}$  from the brine pool, while integrated  
441 oxidation rates in the overlying 2000m water column could only account for  $0.32 \text{ } \mu\text{mol}$   
442  $\text{m}^{-2} \text{ yr}^{-1}$ . These data suggest that a very large component of the diffusive brine pool  
443 methane flux escapes both aerobic and anaerobic oxidation in the water column above the  
444 brine pool and may be released into the atmosphere (or at least subject to dispersion via  
445 lateral advection). These first *in situ* measurements of methane concentration from a  
446 brine pool using the ISMS enabled robust quantification of methane concentrations at *in*  
447 *situ* conditions in these gas-charged brines and reflect the strong influence of the  
448 surrounding hydrocarbon seep environments. Such integrated approaches – wherein  
449 geochemical determinations are coupled with microbiological activity measurements –

450 are the best means of providing a rigorous constraint on methane diffusive fluxes and  
451 transformation rates. This will improve our understanding of the role that hydrocarbon  
452 seeps may play in the delivery of methane into the ocean and ultimately the atmosphere.  
453

453 **Acknowledgements**

454           We are especially grateful to Stephane Hourdez for his immense help with this  
455 instrument during this expedition. We are also grateful to Dr. Charles Fisher for his  
456 support, as well as the captains and crew of the *RV Ronald H. Brown* and *RV Atlantis*.  
457 Special thanks to the pilots and support staff of the *DSV ALVIN* and *DSV JASON II* from  
458 Woods Hole Oceanographic Institution for help collecting and processing samples. An  
459 extra thanks goes especially to Matthew Heinz and Tito Collasius for their assistance in  
460 the machine shop. This research was supported by the U.S. Department of the Interior  
461 Minerals Management Service, the National Oceanic and Atmospheric Administration,  
462 the David and Lucile Packard Foundation, Harvard University, and the National Science  
463 Foundation (MCB-0702504).

464

465

465 **Figure captions**

466 **Figure 1:** Schematic of the in situ mass spectrometer. a) membrane inlet housing, b)  
467 front end plate of titanium pressure housing, c) high pressure solenoid for isolation of  
468 vacuum chamber, d) Alcatel ATH-31+ Turbo Pump, e) vacuum flight tube housing the  
469 SRS Quadrupole RGA-200 including ion source, quadrupoles and detectors f) electronics  
470 head for controlling and reading spectrometer signals g) KNF Neuberger roughing pump  
471 model ANDC-84.3. Sample gas is continuously extracted across the membrane located  
472 in (a) into the high vacuum system (d, g), ionized in (e) and analyzed by the detector and  
473 electronics control unit housed in (f). The instrument is approximately 1m in length.

474

475 **Figure 2:** a) Normalized response at  $m/z$  15 over a range of hydrostatic pressure for  
476 three example fluid temperatures and concentrations,  $10^{\circ}\text{C}$   $1160\mu\text{M}$   $\text{CH}_4$  (grey squares),  
477  $2^{\circ}\text{C}$   $800\mu\text{M}$   $\text{CH}_4$  (black triangles) and  $14^{\circ}\text{C}$   $180\mu\text{M}$   $\text{CH}_4$  (grey triangles). Responses to  
478 pressure were experimentally fit under a wide range of temperatures and concentrations  
479 (as in Bell et al 2007) with values of  $b'$  ranging between 0.02 to 0.24 and values of  $k$   
480 ranging between 0.84 to 0.94. b) The response of  $m/z$  15 (corrected for pressure effects –  
481 see Fig 2a) was linearly proportional to methane concentrations as measured  
482 independently by gas chromatography (grey triangles) and as calculated after Duan et al  
483 2006 during high pressure calibration measurements (black circles).

484

485 **Figure 3:** Photo from the Pilot Cam of ROV Jason showing the starboard manipulator  
486 reaching through the seawater/brine pool interface and sampling at a depth of  
487 approximately 80cm.

488

489 **Figure 4:** a) Depth profile of methane concentration and methane oxidation rates in the  
490 water column above brine pool AC601. Note log scale. Open circles are concentration  
491 measurements made from Niskin bottle samples, while black circles are those made *in*  
492 *situ* using the ISMS. b) Close-up of seawater/brine pool interface and profile into the  
493 brine fluid. Note the linear scale in contrast to panel a. Measured rates of anaerobic  
494 methane oxidation (AOM) at two depths within the brine pool are shown. Note that  
495 these, when corrected for in situ CH<sub>4</sub> concentrations, these rates are 30-45 times higher.  
496 Sulfate concentrations are depleted in the brine, consistent with its role in AOM.



497 **References**

- 498 Bell, R.J., Short, R.T., van Amerom, F.H., Byrne, R.H., 2007. Calibration of an In Situ  
499 Membrane Inlet Mass Spectrometer for Measurements of Dissolved Gases and  
500 Volatile Organics in Seawater. *Environmental Science & Technology* 41 (23),  
501 8123-8128.
- 502 Camilli, R., Hemond, H.F., 2004. NEREUS/Kemonaut, a mobile autonomous underwater  
503 mass spectrometer. *Trends in Analytical Chemistry* 23 (4), 307-313.
- 504 Carini, S., LeClerc, G., Bano, N., Joye, S.B., 2005. Activity, abundance and diversity of  
505 aerobic methanotrophs in an alkaline, hypersaline lake (Mono Lake, CA, USA).  
506 *Environmental Microbiology* 7 (8), 1127-1138.
- 507 Childress, J.J., Arp, A.J., Fisher Jr., C.R., 1984. Metabolic and blood characteristics of  
508 the hydrothermal vent tubeworm *Riftia pachyptila*. *Marine Biology* 83, 109-124.
- 509 Collett, T., Kuuskraa, V., 1998. Hydrates contain vast store of world gas resources. *Oil*  
510 *Gas Journal* 96 (19), 90-95.
- 511 Devol, A.H., 1983. Methane oxidation rates in the anaerobic sediments of Saanich Inlet.  
512 *Limnology and Oceanography* 28, 738-742.
- 513 Dickens, G.R., 2003. Rethinking the global carbon cycle with a large, dynamic and  
514 microbially mediated gas hydrate capacitor. *Earth and Planetary Science Letters*  
515 213 (3-4), 169-183.
- 516 Duan, Z., Mao, S., 2006. A thermodynamic model for calculating methane solubility,  
517 density and gas phase composition of methane-bearing aqueous fluids from 273 to  
518 523K and from 1 to 2000 bar. *Geochimica et Cosmochimica Acta* 70 (13), 3369-  
519 3386.
- 520 Fisher, C.R., Roberts, H., Cordes, E.E., Bernard, B., 2007. Cold seeps and associated  
521 communities of the Gulf of Mexico *Oceanography* 20 (4), 118-129.
- 522 Girguis, P.R., Childress, J.J., Freytag, J.A., Klose, K., Stuber, R., 2002. Effects of  
523 metabolite uptake on proton-equivalent elimination by two species of deep-sea  
524 vestimentiferan tubeworms, *Riftia pachyptila* and *Lamellibrachia luymsi*. *Journal*  
525 *of Experimental Biology* 205, 3005-3006.

526 Girguis, P.R., Lee, R.W., Childress, J.J., Pospesel, M., Desaulniers, N.T., Zal, F.,  
527 Felbeck, H., 2000. Fate of nitrate acquired by the hydrothermal vent tubeworm  
528 *Riftia pachyptila*. Applied and Environmental Microbiology 66 (7), 2783-2790.

529 Girguis, P.R., Orphan, V.J., Hallam, S.J., DeLong, E.F., 2003. Growth and methane  
530 oxidation rates of anaerobic methanotrophic archaea in a continuous flow reactor  
531 bioreactor. Applied and Environmental Microbiology 69, 5492-5502.

532 Hemond, H.F., 1991. A Backpack-portable mass spectrometer for measurement of  
533 volatile compounds in the environment. Review of Scientific Instruments 62 (6),  
534 1420-1425.

535 Johnson, R., Cooks, R., Allen, T., Cisper, M., Hemberger, P., 2000. Membrane  
536 introduction mass spectrometry: Trends and applications Mass Spectrometry  
537 Reviews 19, 1-37.

538 Joye, S.B., Boetius, A., Orcutt, B.N., Montoya, J.P., Schulz, H.N., Erickson, M.J., Lugo,  
539 S., 2004. The anaerobic oxidation of methane and sulfate reduction in sediments  
540 from Gulf of Mexico cold seeps. Chemical Geology 205, 219-238.

541 Joye, S.B., Connell, T.L., Miller, L.G., Oremland, R.S., Jellison, R.S., 1999. Oxidation of  
542 ammonia and methane in an alkaline, saline lake. Limnology and Oceanography  
543 44 (1), 178-188.

544 Joye, S.B., MacDonald, I.R., Montoya, J.P., Peccini, M., 2005. Geophysical and  
545 geochemical signatures of Gulf of Mexico seafloor brines. Biogeosciences 2, 295-  
546 309.

547 Joye, S.B., Samarkin, V., Orcutt, B.N., MacDonald, I.R., Hinrichs, K.-U., Elvert, M.,  
548 Teske, A., Lloyd, K.G., Lever, M.A., Montoya, J.P., Meile, C., 2009. Metabolic  
549 variability in seafloor brines revealed by carbon and sulfur cycling. Nature  
550 Geosciences 2, 349-354.

551 Kaiser, J., Reuer, M.K., Barnett, B., Bender, M.L., 2005. Marine productivity estimates  
552 from continuous O<sub>2</sub>/Ar ratio measurements by membrane inlet mass  
553 spectrometry. Geophysical Research Letters 32, doi:10.1029/2005GL23459.

554 Kana, T.M., Darkangelo, C., Hunt, M.D., Oldham, J.B., Bennett, G.E., Cornwell, J.,  
555 1994. Membrane Inlet Mass Spectrometer for Rapid High-Precision

556 Determination of N<sub>2</sub>, O<sub>2</sub>, Ar in Environmental Water Samples. Analytical  
557 Chemistry 66, 4166-4170.

558 Kana, T.M., Sullivan, M.B., Cornwell, J.C., Groszkowski, K.M., 1998. Denitrification in  
559 estuarine sediments determined by membrane inlet mass spectrometry.  
560 Limnology and Oceanography 43 (2), 334-339.

561 Kennicutt, M.C., II, Brooks, J.M., Denous, G., 1988. Leakage of deep, reservoired  
562 petroleum to the near surface on the Gulf of Mexico continental slope. Marine  
563 Chemistry 24, 29-59.

564 Ketola, R.A., Kotiaho, T., Cisper, M.E., Allen, T.M., 2002. Environmental applications  
565 of membrane introduction mass spectrometry. Journal of Mass Spectrometry 37,  
566 457-476.

567 Kvenvolden, K., 1993. Gas hydrates - geological perspective and global change. Reviews  
568 of Geophysics 31 (2), 173-187.

569 Kvenvolden, K., Lorensen, T.D., 2008. A global inventory of natural gas hydrate  
570 occurrence. <http://walrus.wr.usgs.gov/globalhydrate/index.html>.

571 Lapham, L.L., Alperin, M., Chanton, J., Martens, C.S., 2008. Upward advection rates and  
572 methane fluxes, oxidation, and sources at two Gulf of Mexico brine seeps. Marine  
573 Chemistry 112, 65-71.

574 Lloyd, D., Davies, K.J., Boddy, L., 1986. Mass spectrometry as an ecological tool for in  
575 situ measurement of dissolved gases in sediment systems. FEMS Microbiology  
576 Ecology 38, 11-17.

577 Lloyd, D., Thomas, K.L., Hayes, A., Hill, B., Hales, B.A., Edwards, C., Saunders, J.R.,  
578 Ritchie, D.A., Upton, M., 1998. Micro-ecology of peat: Minimally invasive  
579 analysis using confocal laser scanning microscopy, membrane inlet mass  
580 spectrometry and PCR amplification of methanogen-specific gene sequences.  
581 FEMS Microbiology Ecology 25, 179-188.

582 MacDonald, I.R., Reilly, J., Guinasso, J., Brooks, J.M., Carney, R., Bryant, W.A., Bright,  
583 T.J., 1990. Chemosynthetic mussels at a Brine-filled pockmark in the Northern  
584 Gulf of Mexico. Science 248 (4959), 1096-1099.

585 MacDonald, I.R., Sager, W., Peccini, M., 2003. Association of gas hydrate and  
586 chemosynthetic fauna in mounded bathymetry at mid-slope hydrocarbon seeps:  
587 Northern Gulf of Mexico. *Marine Geology* 198, 133-158.

588 Orcutt, B.N., Boetius, A., Elvert, M., Samarkin, V., Joye, S.B., 2005. Molecular  
589 biogeochemistry of sulfate reduction, methanogenesis and the anaerobic oxidation  
590 of methane at Gulf of Mexico cold seeps. *Geochimica et Cosmochimica Acta* 69  
591 (17), 4267-4281.

592 Oren, A., 2002. Diversity of halophilic microorganisms: environments, phylogeny,  
593 physiology, and applications. *Journal of Industrial Microbiology and*  
594 *Biotechnology* 28, 56-63.

595 Reeburgh, W.S., 1980. Anaerobic methane oxidation: Rate depth distribution in Skan  
596 Bay sediments. *Earth and Planetary Science Letters* 47 (3), 345-352.

597 Reeburgh, W.S., 2007. Oceanic Methane Biogeochemistry. *Chemical Reviews* 107 (2),  
598 486-513.

599 Roberts, H., Carney, R., 1997. Evidence of episodic fluid, gas, and sediment venting on  
600 the northern Gulf of Mexico continental slope *Economic Geology* 92, 863-879.

601 Roberts, H., Fisher, C.R., Bernard, B., Brooks, J.M., Bright, M., Carney, R., Cordes, E.,  
602 Hourdez, S., Hunt, J.J., Joye, S.B., 2007. ALVIN explores the deep northern Gulf  
603 of Mexico Slope. *Eos Transactions* 88, 341-342.

604 Schmidt, M., Botz, R., Faber, E., Schmitt, M., Poggenburg, J., Garbe-Schönberg, D.,  
605 Stoffers, P., 2003. High-resolution methane profiles across anoxic brine-seawater  
606 boundaries in the Atlantis-II, Discovery, and Kebrit Deeps (Red Sea). *Chemical*  
607 *Geology* 200, 359-375.

608 Sloan, L.C., Walker, J.C., Moore, J., TC, Rea, D.K., Zachos, J.C., 1992. Possible  
609 methane-induced polar warming in the early Eocene *Nature* 357, 320-322.

610 Solomon, E.A., Kastner, M., Jannasch, H., Robertson, G., Weinstein, Y., 2008. Dynamic  
611 fluid flow and chemical fluxes associated with a seafloor gas hydrate deposit on  
612 the northern Gulf of Mexico slope. *Earth and Planetary Science Letters* 270, 95-  
613 105.

614 Suess, E., Torres, M., Bohrmann, G., Collier, R., Greinert, J., Linke, P., Rehder, G.,  
615 Trehu, A., Wallman, K., Zuleger, E., 1999. Gas hydrate destabilization: Enhanced

616 dewatering, benthic material turnover and large methane plumes at the Cascadia  
617 convergent margin. *Earth and Planetary Science Letters* 170, 1-15.

618 Tortell, P., 2005a. Small-scale heterogeneity of dissolved gas concentrations in marine  
619 continental shelf waters. *Geochemistry, Geophysics, Geosystems* 6, Q11M04.

620 Tortell, P.D., 2005b. Dissolved gas measurements in oceanic waters made by membrane  
621 inlet mass spectrometry. *Limnology and Oceanography: Methods* 3, 24-37.

622 Valentine, D.L., Blanton, D., Reeburgh, W.S., Kastner, M., 2001. Water column  
623 methane oxidation adjacent to an area of active hydrate dissociation, Eel River  
624 Basin. *Geochimica et Cosmochimica Acta* 65, 2633-2640.

625 Zachos, J.C., Pagani, M., Sloan, L., Thomas, E., Billups, K., 2001. Trends, rhythms and  
626 aberrations in global climate 65 Ma to Present. *Science* 292 (5517), 686-674.

627

628

629

630

631

632

633

Table 1: Major chemical components of brine pool AC601

| Depth cm | pH   | salinity | oxygen | Concentration mM |                  |                               |                 |                              |                              |                              | Concentration mM |        |        |      |       |         |  |  |  |  |  |  |     |  |
|----------|------|----------|--------|------------------|------------------|-------------------------------|-----------------|------------------------------|------------------------------|------------------------------|------------------|--------|--------|------|-------|---------|--|--|--|--|--|--|-----|--|
|          |      |          |        | DIC              | H <sub>2</sub> S | SO <sub>4</sub> <sup>-2</sup> | Cl <sup>-</sup> | CH <sub>4</sub> <sup>a</sup> | CH <sub>4</sub> <sup>b</sup> | NH <sub>4</sub> <sup>+</sup> | NO <sub>x</sub>  | DIN    | TDN    | DON  | DOC   | DOC:DON |  |  |  |  |  |  |     |  |
| 5        |      |          |        |                  |                  |                               |                 |                              |                              | 14.35                        |                  |        |        |      |       |         |  |  |  |  |  |  |     |  |
| 20       | 6.29 | 82       | <2 μM  | 11.2             | 0.00             | 20                            | 1366            | 0.454                        | 20.29                        | 1750                         | 3.4              | 1753.4 | 1843.5 | 90.1 | 423.5 |         |  |  |  |  |  |  | 4.7 |  |
| 80       |      |          |        |                  |                  |                               |                 |                              |                              | 33.29                        |                  |        |        |      |       |         |  |  |  |  |  |  |     |  |
| 100      | 6.25 | 92       | <2 μM  | 12.8             | 0.25             | 16                            | 1533            | 1.320                        | 38.40*                       | 2195                         | 0.3              | 2195.3 | 2280.5 | 85.2 | 380.0 |         |  |  |  |  |  |  | 4.5 |  |

<sup>a</sup>Concentrations measured via gas chromatography on samples retrieved with a CTD rosette and Niskin bottles

<sup>b</sup>Concentrations measured via *in situ* mass spectrometer

\* estimated by regression of the three ISMS data points collected above

635  
636  
637

Table 2: Rates of sulfate reduction and anaerobic methane oxidation in Gulf of Mexico brine pool AC601

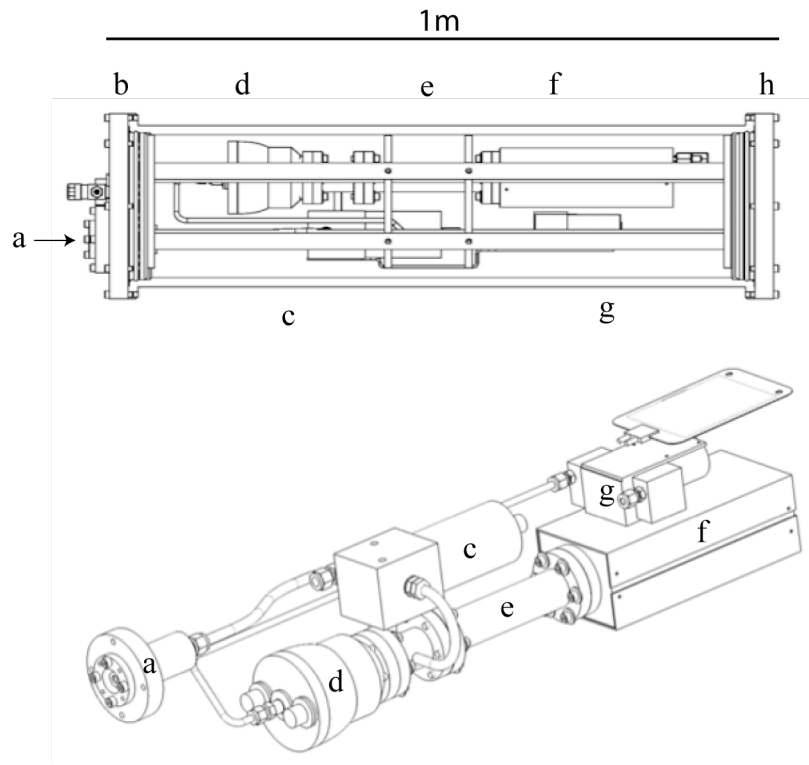
| Depth cm | Rate nM/d         |                              |  |
|----------|-------------------|------------------------------|--|
|          | Sulfate Reduction | Anaerobic Methane Oxidation* | Anaerobic Methane Oxidation <sup>^</sup> |
| 20       | 107.1 ± 14.6      | 78.8 ± 7.6                   | 3502.0 ± 340                             |
| 100      | 49.8 ± 8.4        | 62.1 ± 13.1                  | 1807.4 ± 330                             |

\* measured using water samples collected via CTD rosette and Niskin bottles

<sup>^</sup> estimated rates corrected for measured concentrations *in situ* and using rate constants measured from shipboard incubations of brine pool water collected via Niskin bottles

638  
639  
640  
641  
642  
643

643



Wankel Figure 1

644

645

646

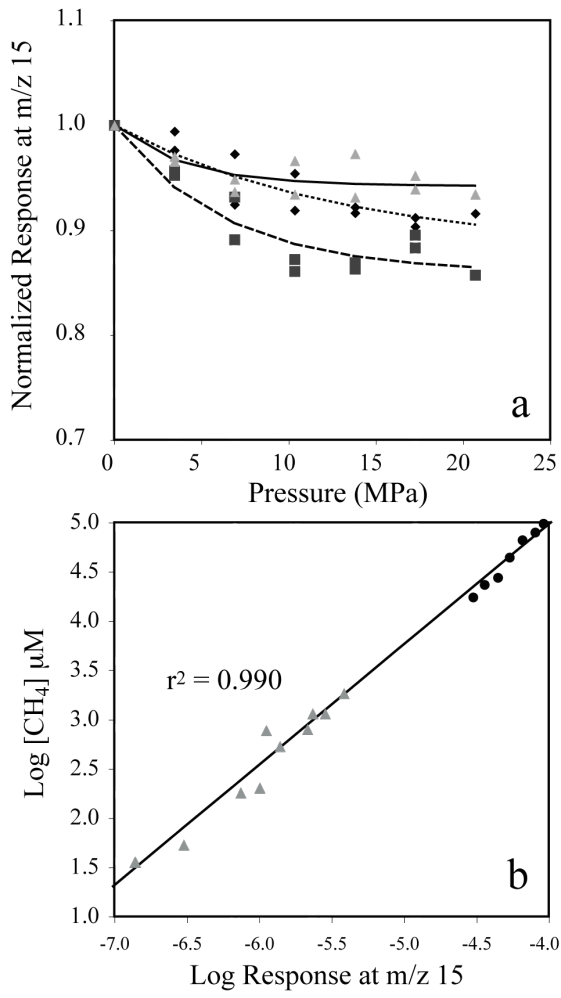
647

648

649



649



650

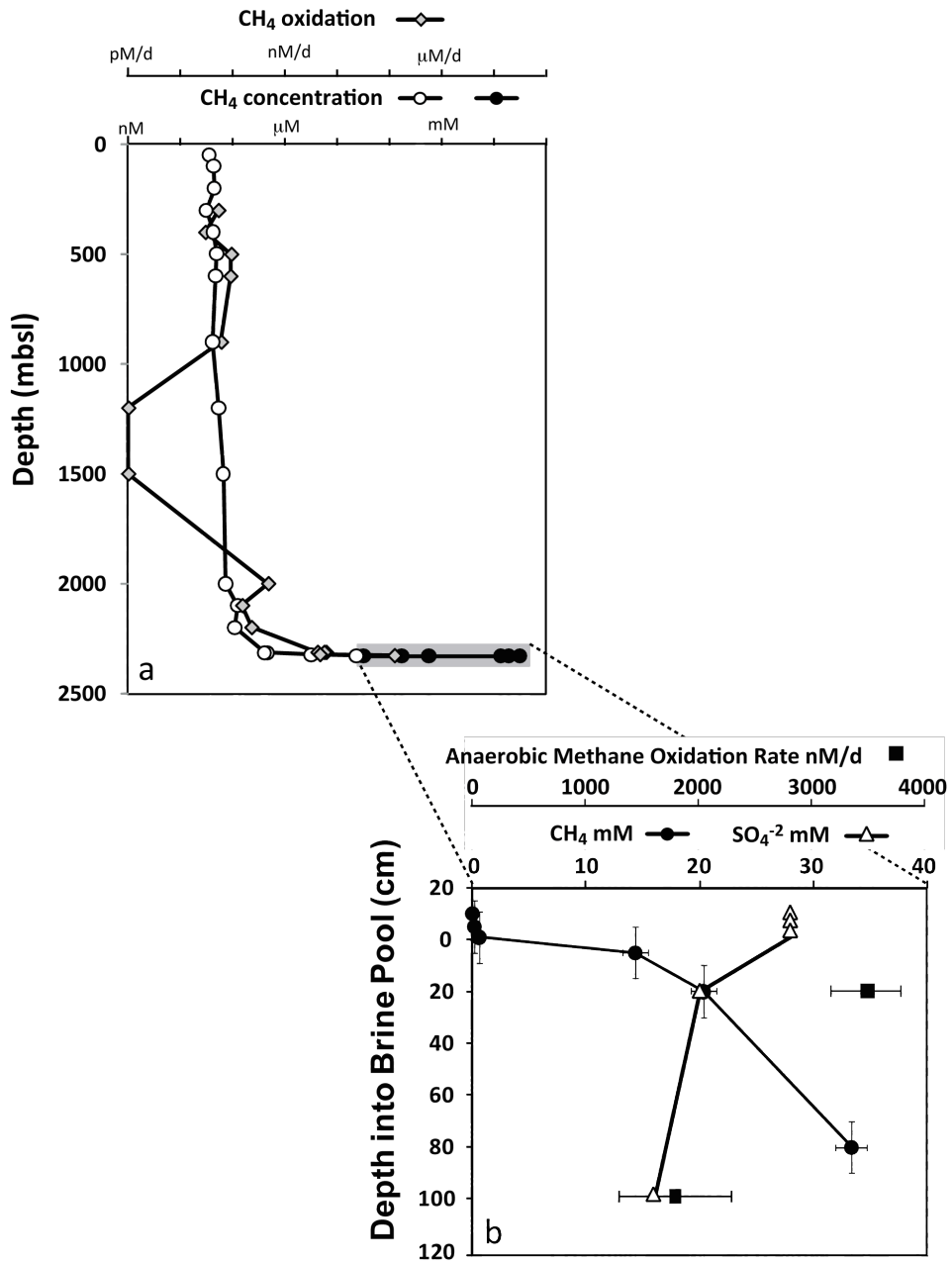
Wankel Figure 2

651  
652

### Wankel Figure 3



653



654  
 655  
 656

Wankel Figure 4